INTERNATIONAL JOURNAL FOR NUMERICAL METHODS IN FLUIDS, VOL. 18, 669–694 (1994)

A NET INFLOW METHOD FOR INCOMPRESSIBLE VISCOUS FLOW WITH MOVING FREE SURFACE

S. P. WANG AND K. K. WANG

Sibley School of Mechanical and Aerospace Engineering, Cornell University, Ithaca, NY 14853, U.S.A.

SUMMARY

A new finite element procedure called the net inflow method has been developed to simulate time-dependent incompressible viscous flow including moving free surfaces and inertial effects. As a fixed mesh approach with triangular element, the net inflow method can be used to analyse the free surface flow in both regular and irregular domains. Most of the empty elements are excluded from the computational domain, which is adjusted successively to cover the entire region occupied by the liquid. The volume of liquid in a control volume is updated by integrating the net inflow of liquid during each iteration. No additional kinetic equation or material marker needs to be considered. The pressure on the free surface and in the liquid region can be solved explicitly with the continuity equation or implicitly by using the penalty function method. The radial planar free surface flow near a 2D point source and the dam-breaking problem on either a dry bed or a still liquid have been analysed and presented in this paper. The predictions agree very well with available analytical solutions, experimental measurements and/or other numerical results.

KEY WORDS Free surface Finite element Viscous flow

INTRODUCTION

Incompressible viscous flow with moving free surfaces has drawn broad attention because of its important applications in environmental engineering, die casting, polymer processing and many other areas of interest. Owing to the presence of the moving free surface, analytic solutions to such problems are typically limited to only one-dimensional cases. Experimentation and prior experience had been the main tools for treating such problems until the mid-1960s when numerical solutions[1] became available. Generally, numerical methods for free surface problems can be divided into two groups based upon whether the mesh is moving or fixed after the initial input. Ideally, it is preferred that the free surface always lies on the mesh boundaries to avoid any discontinuities between the mesh points. When using the fixed mesh approach, the position of the free surface has to be interpolated between the mesh points and either an explicit or implicit smoothing of the discontinuities is required along such surfaces. On the other hand, the moving mesh solutions are typically confined to special applications owing to limitations in the rezoning technique. Accordingly, the fixed mesh approach is still the more appropriate means of handling general time-dependent free surface flows.

For steady state problems most of the available methods manage to modify the mesh. Nickell *et al.*,[2] Omodei[3] and Silliman and Scriven[4] released one boundary condition on the free surface and adjusted the initial free surface position and the corresponding mesh successively until all

CCC 0271–2091/94/070669–26

Received 10 March 1993
Revised 3 August 1993

boundary conditions were satisfied. Ruschak[5] and Saito and Scriven[6] took the free surface position as a degree of freedom in order to reduce the number of iterations. Ryskin and Leal[7] generated an orthogonal co-ordinate such that all boundaries of the domain coincided with the co-ordinate line in two-dimensional axisymmetric space.

For unsteady problems, Kheshgi and Scriven[8] tracked the free surface position along preselected spines. Since the filling pattern is unknown, it may be difficult to generate appropriate spines before the problem is solved. Another moving mesh approach for unsteady problems is better known as the Lagrangian formulation. In this approach, the mesh points are treated as material points and the mesh varies according to the motion of the liquid. A close variant of this approach called the arbitrary Lagrangian–Eulerian method[9,10] was developed to handle possible mesh entanglement caused by material distortions. Whenever general motion of free surfaces is required, however, the fixed mesh approach seems to be a more viable candidate. Harlow and Welch[11] solved the Navier–Stokes equations in Eulerian co-ordinates and tracked the motion of markers originally distributed in the liquid cell as material points (MAC) to locate the new position of the free surfaces. In simulating the injection-moulding process, Broyer *et al.*[12] first defined the free surface position by means of a fractional volume of liquid, f, which is unity in regions completely occupied by liquid, lies between zero and unity near the front position and is zero otherwise. Hirt and Nichols[13] expressed the mass conservation for an incompressible liquid in terms of the fractional volume of fluid (VOF) and obtained the kinetic equation

$$\frac{\partial f}{\partial t} + u\frac{\partial f}{\partial x} + v\frac{\partial f}{\partial y} = 0. \tag{1}$$

MAC and VOF are quite similar to each other and both can be applied in three-dimensional computations. However, there are concerns about the conservation of mass near the free surface. According to the definition in MAC,[1,11] cells without marker particles are considered empty. Non-empty cells lying adjacent to empty cells are surface cells and all other cells with marker particles are considered filled. Similar definitions are used in VOF,[13] with the exception that the number of marker particles is replaced by the fractional volume of liquid. From such definitions, however, it follows that cells considered as being filled by liquid may not actually be filled. For instance, a partially filled cell may be surrounded by non-empty cells and be considered filled. In both methods the position of the free surface is updated after iterations on the momentum and continuity equations have converged. As a result, mass conservation can be satisfied only when the free surface recedes. If the free surface advances, empty or partially filled cells may actually become overfilled. Whenever a non-empty cell becomes filled or surrounded by other non-empty cells, the computational domain changes and the free surface boundary conditions have to be applied at the new location of the interface in the following time step. This sudden change may cause numerical instability or unphysical results for the velocity and pressure fields near the interface. After all, tracking the marker position is helpful in determining the new free surface location but the extrapolation of the marker position does not satisfy mass conservation. When a non-uniform mesh is used with VOF, a mesh point is not necessarily the geometric centre of the corresponding control volume. In this case the momentum advection becomes inaccurate[13] and such an error accumulates with respect to time.

In this paper we consider the incompressible flow of a Newtonian liquid which is in direct contact with the air. It is well understood that by considering the interface to be traction-free (except for a uniform atmospheric pressure), the problem can be solved efficiently without including the motion of the air. However, this approach is convenient only for the moving mesh

method in which the nodes are considered as material points that move with the liquid. When using a fixed mesh approach without considering the air, the velocity in elements crossing the interface cannot be determined, since part of the element is located in the undefined region. Also, it would be difficult to update the advancing free surface position since extrapolation into the undefined domain would be required. On the other hand, if both the liquid and the air are considered, more computational effort is required and there are discontinuities across the interface. These discontinuities exist in the pressure, velocity gradient and material properties.

In our approach, the motion of both the liquid and a layer of air near the interface are considered based upon a fixed mesh approach. The volume of incompressible liquid in each control volume is calculated by directly integrating the net inflow rate of the liqud with respect to time. The governing equations will be derived below followed by the numerical algorithm. For verification, the radial planar free surface flow near a 2D point source as well as the dam-breaking problem on either a dry bed or a still liquid will be analyzed. The results will be compared with analytical solutions, experimental measurements and/or other numerical solutions whenever available.

GOVERNING EQUATIONS

When both the liquid and the air are considered, the equations governing the non-linear system are as follows:

incompressible liquid,

$$\nabla \cdot \mathbf{v} = 0, \tag{2}$$

$$\rho_1 \frac{\partial \mathbf{v}}{\partial t} = -\rho_1(\mathbf{v} \cdot \nabla)\mathbf{v} - \nabla p + \mathbf{b} + \mu_1 \nabla^2 \mathbf{v}; \tag{3}$$

air,

$$\frac{\partial \rho_{\text{air}}}{\partial t} + (\nabla \cdot \rho_{\text{air}} \mathbf{v}) = 0, \tag{4}$$

$$\rho_{\text{air}} \frac{\partial \mathbf{v}}{\partial t} = -\rho_{\text{air}}(\mathbf{v} \cdot \nabla)\mathbf{v} - \nabla p + \mu_{\text{air}} \nabla^2 \mathbf{v}, \tag{5}$$

$$\rho_{\text{air}} = p/RT. \tag{6}$$

For the two-dimensional case the associated interfacial boundary conditions are

$$\left(-p + 2\mu \frac{\partial u_n}{\partial x_n}\right)_l = \left(-p + 2\mu \frac{\partial u_n}{\partial x_n}\right)_{\text{air}}, \tag{7}$$

$$\mu_l \left(\frac{\partial u_n}{\partial x_t} + \frac{\partial u_t}{\partial x_n}\right)_l = \mu_{\text{air}} \left(\frac{\partial u_n}{\partial x_t} + \frac{\partial u_t}{\partial x_n}\right)_{\text{air}}, \tag{8}$$

$$(u_n)_l = (u_n)_{\text{air}}, \tag{9}$$

$$(u_t)_l = (u_t)_{\text{air}}. \tag{10}$$

In the above equations, t, u, v, p, ρ and μ denote time, velocity components in the x- and y-direction, pressure, density and dynamic viscosity respectively. R and T are the gas constant and the absolute temperature respectively. Subscripts 'l' and 'air' refer to the liquid and air

regions respectively, while subscripts 't' and 'n' denote the tangential and normal directions of the interface respectively. In addition, $\mathbf{v}$ and $\mathbf{b}$ denote the velocity vector and a possible body force acting on the liquid respectively. The surface tension on the interface is not included in this study.

It should be noted that although the stresses are continuous across the interface, the pressure and velocity gradient are discontinuous owing to different material properties. Since the density and dynamic viscosity of the air are much smaller than those of the liquid, the viscous stresses on the interface have negligible influence on the motion of the liquid. This is the reason why the interface is often referred to as a 'free' surface. In this study the following assumptions are made.

1. The pressure of the air is uniform.
2. The kinematic viscosity of the air is equal to that of the liquid.

From the momentum equation, it follows that the pressure gradient balances either the inertial force of the viscous effects, whichever is the larger. However, the motion of the air has little influence on the liquid and we are interested only in the motion of the liquid. Neglecting the pressure gradient in the air seems to be acceptable in this case. For the same reason, it should not make any difference whether we consider the real air or any other gas with very low density and small dynamic viscosity. Therefore, in the numerical analysis, the air is replaced by a pseudo-gas. The density ρ_p, and dynamic viscosity μ_p of the pseudo-gas are much smaller than those of the liquid but its kinematic viscosity is taken to be the same as that of the liquid. With these assumptions the equations governing the liquid motion do not change but the governing equations of the pseudo-gas become

$$p = p_0, \tag{11}$$

$$\rho_l \frac{\partial \mathbf{v}}{\partial t} = -\rho_l(\mathbf{v} \cdot \nabla)\mathbf{v} + \mu_l \nabla^2 \mathbf{v}, \tag{12}$$

where the continuity equation is not needed to determine the velocity of the pseudo-gas because the pressure is assumed to be uniform. Also, we have multiplied a coefficient ($= \rho_l/\rho_p = \mu_l/\mu_p$) on both sides of the momentum equation such that the material constants become the same as those of the liquid. This can be done because the pseudo-gas is assumed to have the same kinematic viscosity as the liquid.

Since the viscous effect of the pseudo-gas is negligibly small when compared with that of the liquid, the shear stress τ and normal stress σ_n of the liquid on the interface must be equal to zero and the pressure of the pseudo-gas, p_0 respectively, i.e.

$$\sigma_n = -p_l + 2\mu_l \frac{\partial u_n}{\partial x_n} = -p_0, \qquad \tau = 0. \tag{13}$$

On the other hand, (9) and (10) can now be written as

$$\mathbf{v}_p = \mathbf{v}_l. \tag{14}$$

The meaning of (13) is that the liquid does not 'feel' any resistance from the pseudo-gas except the uniform pressure. On the other hand, the pseudo-gas is driven by the liquid on the interface owing to the no-slip condition (14).

From (13), the liquid pressure on the interface can be determined if the free surface position and the liquid distribution are known. Since there is a coupling relation between the liquid

pressure and the continuity equation (2), it seems that there are two constraints on the liquid pressure on the interface. However, it should be kept in mind that there is another unknown, namely the position of the free surface. In other words, if the interfacial position can be considered as one unknown, the number of unknowns matches the number of constraints on the free surface. Intuitively, the number of unknowns of the interfacial position in a multidimensional space is more than one. This is the reason why Kheshgi and Scriven[8] determined the interfacial position along preselected lines so that there is only one unknown on each line. A more flexible solution was suggested by Broyer *et al.*,[12] who defined a scalar function called the fractional volume of liquid. Ideally, the fractional volume is unity in the region occupied by liquid and zero elsewhere. If the scalar field of the fractional volume is known, the position of the interface can be determined. In order to obtain the fractional function, Hirt and Nichols[13] solved the kinetic equation (1). However, since the interfacial position and the liquid pressure on the interface can be solved directly by satisfying the free surface boundary condition and the incompressibility constraint, the kinetic equation (1) is actually unnecessary.

FINITE ELEMENT DISCRETIZATION

The present net inflow method is based on the six-noded triangular finite element originally developed by Baliga and Patankar.[14] Prakash[15] improved the numerical stability of the

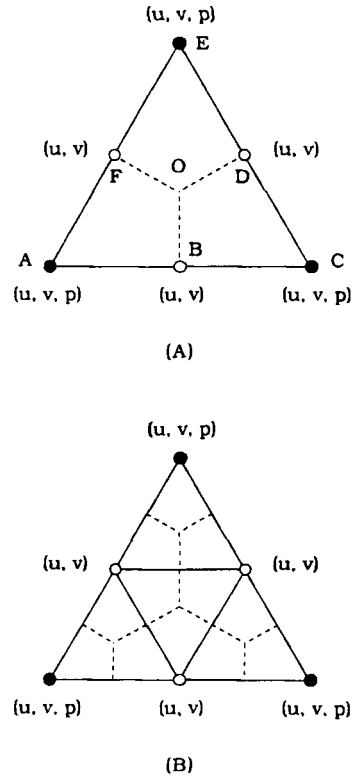

Figure 1. (A) Six-noded control volume finite element and variables at each node. Dashed lines are boundaries of mass control volume. (B) Same as (A) except that solid and dashed lines are boundaries of subelements and momentum control volumes respectively

procedure by incorporating the donor-cell upwind algorithm proposed by Schneider and Raw.[16] However, if the aspect ratio of the elements is large (e.g. two) or the flow direction is parallel to one or more control volume boundaries, the donor-cell upwind method itself may cause numerical instability. The solution to these problems has been discussed elsewhere.[17] As shown in Figure 1(A), the triangular element includes six nodes, namely three at the vertices and three at the midpoints of the sides. There are two velocity components at each node and the pressure is calculated only at the vertex nodes.

As shown in Figure 1(B), an element is divided into four subelements by joining the middle nodes. The pressure is considered linear on each primary element whereas the velocity is interpolated linearly on each subelement. When considering the mass conservation of the liquid, each primary element is divided into three sub-mass control volumes (SMasCVs) by drawing lines from the centroid to the midpoint of each side, as indicated in Figure 1(A). After an irregular domain is discretized with the triangular elements, as seen in Figure 2(A), the SmasCVs attached to the same vertex node constitute a mass control volume (MasCV). Such MasCVs may be

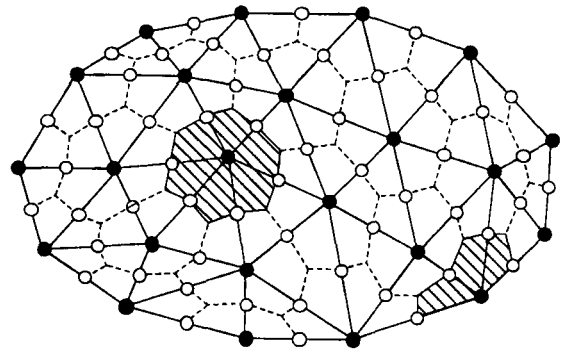

(A)

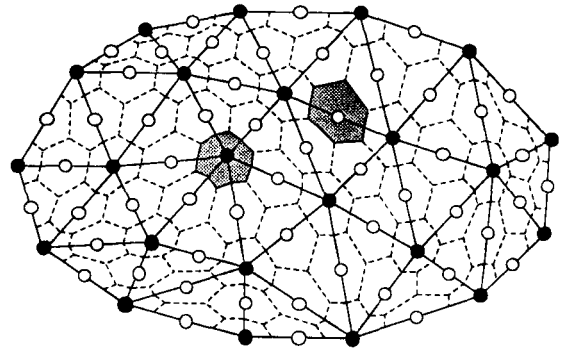

(B)

Figure 2. (A) Typical triangular discretization of an irregular doman and indication of mass control volumes. (B) Same domain as in (A) but with momentum control volumes indicated

composed of one, two or more SMasCVs, depending on the number of elements containing the corresponding vertex node. For a given mesh, a flexible combination of these SMasCVs is much better than the whole MasCVs in fitting the irregular shape of the free surface. However, a special algorithm will be required to enforce the incompressibility constraint on the velocity in an MasCV in which not all its SMasCVs are filled. For handling momentum equilibrium, each of the subelements is divided into three quadrilaterals, as shown in Figure 1(B). A momentum control volume (MomCV) is a polygon, as shown in Figure 2(B), composed of the quadrilaterals associated with each given node. Unlike the MasCVs, the MomCVs will not be divided into smaller units in the numerical procedure.

NET INFLOW METHOD

The major difficulty in a free surface flow problem is that the interfacial position, which does not appear explicitly in the governing equations as a variable, is unknown. However, the free surface boundary conditions on the interface in (13) cannot be satisfied simultaneously with the continuity equation of the liquid unless they are applied in the appropriate domain. In other words, the interfacial position can be determined by adjusting its initial position successively such that all the conservation equations and free surface boundary conditions are satisfied simultaneously. For a fixed mesh method, it is inevitable that some of the elements or control volumes may be located across the interface. This implies that the conservation equations and the free surface boundary conditions can only be satisfied approximately. In this work, the exact position of the interface is not required for the numerical procedure. It is determined only to display the predicted solution.

At the beginning of a time step, the initial condition or the result from the previous time step is used as the initial guess. Based on the distribution of the liquid, all the SMasCVs are divided into three categories: filled, partially filled or empty. Equations (2) and (3) are applied in those subelements associated with the filled SMasCVs. For those subelements in the partially filled region, equations (11) and (12) are employed. The interfacial boundary conditions (13) and (14) are applied on the nodes attached to both filled and partially filled SMasCVs. Most of the empty region is excluded from the computational domain to reduce the computational effort. After each iteration the volume of liquid in each SMasCV is updated. If the solution is correct, all SMasCVs filled by liquid should have been included in the filled region. Any violation means that the mass conservation of the liquid is not properly satisfied and the computational domain should be corrected based on the updated status of the control volumes. In other words, the approximate interfacial position is approached successively by adjusting the region where the incompressibility constraint and the free surface boundary conditions should be applied. The implementation of the numerical procecure is illustrated as follows.

Volume of liquid in SMasCV

The instantaneous volume of liquid in an SMasCV is the sum of its initial volume and the net inflow of the liquid from the beginning till then. In an SMasCV, e.g. ABOF in Figure 1(A), the net inflow rate is the sum of the volumetric flow rate through its four boundaries, namely AB, BO, OF and FA. The volume inflow rate of fluid across each boundary can be expressed as

$$\dot{q} = (\mathbf{v}_c \cdot \mathbf{n}_i)L, \tag{15}$$

where L, $\mathbf{v}_c$ and $\mathbf{n}_i$ are the length of the boundary, the velocity vector at the centre of the boundary and the inward unit vector perpendicular to the boundary respectively. As an implicit scheme,

the velocity at the end of a given time step is used in (15). It should be noted that the fluid flowing across a boundary is not necessarily liquid or air. In order to determine the actual amount of liquid flowing into the SMasCV, an effective flowing time δt will be defined such that the volume of liquid flowing across a boundary during a time step is

$$\Delta q = \dot{q} \times \delta t. \tag{16}$$

The total volume of liquid in an SMasCV at the end of the ith iteration of a time step k is updated by adding the net inflow of liquid through its boundaries and is expressed as

$$q_i^k = q^{k-1} + \sum_{n=1}^{m} \Delta q_n, \tag{17}$$

where m is the number of boundaries with non-zero effective flowing time. If q_i^k is zero, the corresponding SMasCV is considered empty. If q_i^k is larger than zero but smaller than the total volume of the SMasCV, Q, the SMasCV is partially filled. Otherwise the SMasCV is filled. It should be noted that the volume of liquid in a partially filled SMasCV should be updated after each iteration by using (17). It is possible that the calculated volume of liquid in a partially filled SMasCV may exceed its available volume during a given iteration. This simply means that the velocity in this SMasCV has not converged and the iteration should continue after the computational domain is adjusted, as discussed further below.

Effective flowing time

During a time step, the fluid flowing through the boundary may be air, liquid or both, depending on when the liquid reaches the boundary. This means that the effective flowing time of the liquid, δt, at a boundary may be equal to or less than the time step Δt. If δt is always taken to be Δt, the magnitude of the velocity on the free surface will not be correct since the volume of liquid flowing across the boundary is limited. At the beginning of a time step, an effective flowing time is assigned to each SMasCV. The effective flowing time is Δt if the SMasCV is filled and zero otherwise. After each iteration the volume of liquid in each empty or partially filled SMasCV within the computational domain is updated. If the volume of liquid in an SMasCV, q^{k-1}, is less than the total volume of the SMasCV, Q, at the beginning of a given time step, k, and the updated volume, q_i^k, becomes equal to or larger than the total volume after the ith iteration, the effective flowing time of this SMasCV should be updated as

$$\delta t = \Delta t\left(1 - \frac{Q - q^{k-1}}{q_i^k - q^{k-1}}\right). \tag{18}$$

The effective flowing time for a boundary is simply equal to the larger effective flowing time of the two SMasCVs on either side of the boundary.

Computational domain

An element with all three of its SMasCVs empty is designated an empty element. In each iteration, these empty elements are excluded from the computational domain, except for those sharing nodes with non-empty elements. As a result, a layer of empty or partially filled elements near the interface and all the filled elements are included in the computational domain, which

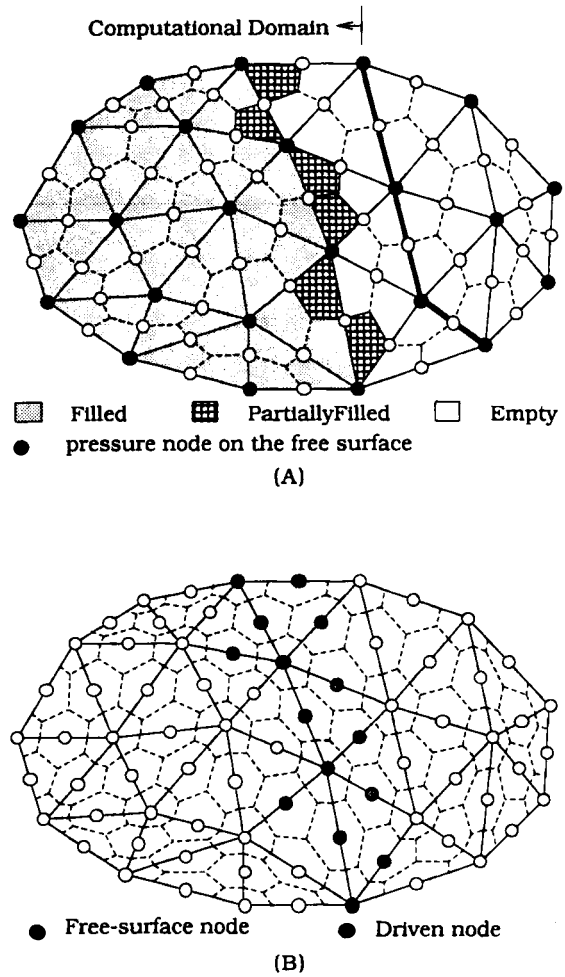

Figure 3. (A) Typical computational domain. (B) Corresponding free surface and driven nodes based on status in (A)

is updated after each iteration. As shown in Figure 3(A), the computational domain in this case has been divided into 31 primary triangular elements. Based on the given distribution of the liquid and the geometry of the mesh, each SMasCV can be categorized as being either filled, partially filled or empty. In turn, if a node is surrounded by only filled SMasCVs, it is considered to be an interior node. All other nodes within the computational domain are considered to be exterior nodes. These exterior nodes are further divided into several groups such that the free surface boundary condition can be applied. In particular, the exterior nodes associated with filled SMasCVs are known as free surface nodes. The other exterior nodes immediately adjacent to the free surface nodes are called driven nodes. These definitions will be used in the implementation of the interfacial boundary conditions. In Figure 3(B) the free surface nodes and driven nodes have been determined based on the status of the SMasCVs given in Figure 3(A).

Conservation of mass

In a control volume filled with liquid, the continuity equation (1) can be integrated and approximated as

$$\sum_{i=1}^{m} \Delta q_i = 0, \tag{19}$$

where m is the number of linear boundaries surrounding the control volume. Obviously, (19) will fail if the control volume is not completely filled by the liquid. As defined earlier, an MasCV is composed of several SMasCVs. If none of these SMasCVs is filled, the pressure within the MasCV is considered to be that of the empty region and no mass conservation for the liquid is required. If one or more SMasCVs in an MasCV are filled, the velocity within these filled SMasCVs should be divergence-free such that the conservation of mass is satisfied. In the following, two methods, namely the discrete migration scheme (DMS) and the continuous interpolation scheme (CIS), will be proposed to handle this problem.

As shown in Figure 4, an irregular domain has been divided into three primary triangular elements ABC, BDC and BED. At the beginning of the present time step suppose that SMasCV B_1 is filled, A_1, B_2 and C_1 are partially filled and all the others are empty. During this time step a given volume of liquid Δq_{in}, flows into SMasCV B_1 from outside. In the discrete migration scheme, the incompressibility constraint is enforced only within the filled SMasCVs. According to this approach, the mass conservation during the first iteration of the present time step needs to be considered only in B_1 as follows:

$$\Delta q_{in} + \Delta q_{a1,b1} + \Delta q_{c1,b1} + \Delta q_{b2,b1} = 0, \tag{20}$$

where the subscripts denote the SMasCVs associated with the boundaries across which the liquid flows. Note that the liquid volume is taken to be positive if it flows into SMasCV B_1. After the first iteration, the volume of liquid in A_1, B_2 and C_1 should be updated according to the methods described above. If none of them becomes filled, then the iteration continues without any change in the computational domain. However, some of the partially filled SMasCVs will eventually become filled. If, for instance, SMasCVs B_2 and A_1 are found to be filled during a particular iteration, the incompressibility constraint should be updated accordingly. In MasCV A, the net inflow of the liquid must be equal to the volume of the void in the control volume, i.e.

$$\Delta q_{b1,a1} + \Delta q_{c1,a1} = Q_{a1} - q_{a1}, \tag{21}$$

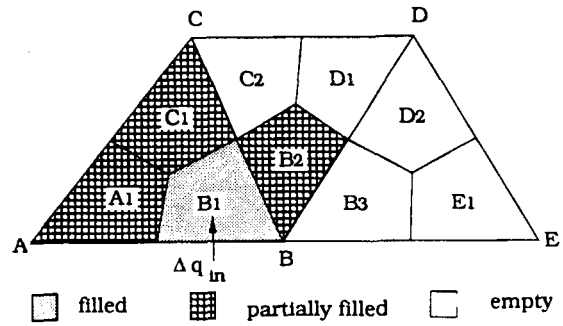

Figure 4. Mass conservation in a mass control volume with filled, partially filled and empty submass control volumes

where q_{a1} denotes the volume of liquid in A_1 at the beginning of the current time step. It should be noted that in (20) and (21), $\Delta q_{b1,a1}$ and $\Delta q_{a1,b1}$ denote the same volume but of opposite sign. Similarly, the net inflow of the liquid in SMasCVs B_1 and B_2 has to equal the void in B_2, i.e.

$$\Delta q_{in} + \Delta q_{a1,b1} + \Delta q_{c1,b1} - (\Delta q_{b2,c2} + \Delta q_{b2,d1} + \Delta q_{b2,b3}) = Q_{b2} - q_{b2}. \tag{22}$$

Since B_1 and B_2 belong to the same MasCV, the liquid flowing through the boundary between B_1 and B_2 does not have to be considered in (22). The same procedure is repeated if any other SMasCVs become filled during the following iteration.

As the distribution of the liquid changes in the domain, the computational domain and the incompressible region migrate accordingly but discretely. The resulting discrete migration scheme is very simple and easy for numerical implementation. However, for a highly non-linear problem, a sudden change in the computational domain and boundary conditions increases the required number of iterations and the possibility of divergence. On the other hand, an SMasCV is considered unfilled even if the volume of liquid is very close to but still less than its total volume. In practical applications, this means that the numerical solutions may be mesh-dependent and sensitive to the truncation limit. In the continuous interpolation scheme the liquid flowing between the filled and partially filled SMasCVs within the same MasCV is interpolated linearly. For example, in (20) the liquid volume $\Delta q_{b2,b1}$ flowing from B_2 to B_1 is replaced by an interpolated volume defined as

$$\Delta q_{b2,b1,int} = (1 - f_{b2})\,\Delta q_{b2,b1} - f_{b2}(\Delta q_{b2,c2} + \Delta q_{b2,d1} + \Delta q_{b2,b3}), \tag{23}$$

where f_{b2} is the volume fraction of liquid in B_2. It can be seen easily that (23) offers a smooth transition between (20) and (22). As a result, the continuous interpolation scheme is more stable and its solution is less mesh-dependent.

The continuity equations (20)–(22) can be solved explicitly with the pressure or implicitly using the penalty function method. For example, when using the implicit method, the continuity equation (20) and the corresponding liquid pressure are combined with the penalty function defined as

$$p_B = \frac{\Delta q_{in} + \Delta q_{a1,b1} + \Delta q_{c1,b1} + \Delta q_{b2,b1}}{\varepsilon_p Q_{b1}}, \tag{24}$$

where ε_p is the penalty factor, which can be any positive number much smaller than unity but still much larger than the truncation limit of the computer. When compared with the explicit method or other iterative solutions, e.g. the SIMPLE[18] algorithm, the penalty function reduces the number of unknowns (pressure) and still offers fast convergence. However, the penalty factor must be small. If it is large, the compressibility error increases. On the other hand, the round-off error may become significant if the penalty factor is close to the truncation limit of the computer. In the proposed expression (24) the compressibility error in the numerator is normalized by the control volume such that the percentage of the compression error is independent of the element size. For the problems we have tested, a penalty factor between 10^{-4} and 10^{-7} seems to be appropriate. Details of the fundamental principles and the error estimate of the penalty function can be found elsewhere.[19–24] When the status of the SMasCVs in an MasCV changes, the corresponding pressure can still be expressed using the penalty function. Similarly to (24), (21) can be expressed by the penalty function as

$$p_A = \frac{\Delta q_{b1,a1} + \Delta q_{c1,a1} - Q_{a1} + q_{a1}}{\varepsilon_p Q_{a1}}. \tag{25}$$

Momentum equilibrium

For momentum equilibrium, equation (3) is integrated in each momentum control volume. The resulting equation can be rearranged using the divergence theory and expressed as

$$A\rho_l(\mathbf{v}_i^k - \mathbf{v}^{k-1}) + \Delta t \sum_{j=1}^{m} [\rho_l(\mathbf{v}_{i-1,j}^k \cdot \mathbf{n}_o)\mathbf{v}_{i,j}^k + p_j \mathbf{n}_o - \mu_l(\mathbf{n}_o \cdot \nabla \mathbf{v}_i^k)]L_j = \Delta t A \mathbf{b}, \tag{26}$$

where superscript k and subscripts i and j denote the kth time step, the ith iteration and the jth boundary respectively. A, m and $\mathbf{n}_o$ are the area of the MomCV, the total number of linear boundaries surrounding the MomCV and the outward unit vector perpendicular to each boundary respectively. Since the body force and pressure are the only differences between (3) and (10), equation (26) is applicable for the whole computational domain, except that the pressure and body forces need to be integrated only when they are non-zero. In order to avoid the numerical instability at high Reynolds number, the velocity in the non-linear advective terms is determined by the donor cell upwind method.[15] For better convergence, the momentum equilibrium equation and the continuity equation should be solved simultaneously with the Newton–Raphson method. When using the penalty function method, the pressure in (26) is replaced by the penalty function (24) or (25).

Interfacial boundary conditions

For the interfacial boundary conditions (13) and (14), the free surface nodes are considered on the liquid side and the driven nodes on the air side of the interface. The no-slip boundary condition (14) and the zero-shear-stress boundary condition in (13) are implemented by forcing the velocity at the driven nodes to follow the liquid velocity at the free surface nodes. To achieve this, the viscous force between the free surface nodes and the driven nodes is multiplied by a large constant $1/\varepsilon_v$ when integrating on the driven nodes. On the other hand, this viscous force is excluded when integrating the forces on the free surface nodes. As a result, the liquid velocity at the free surface nodes is not affected by the viscous diffusion from the pseudo-gas and the pseudo-gas velocity at the driven nodes follows the liquid velocity at the free surface nodes closely. The penalty factor, ε_v, multiplying the viscous force should be positive and much smaller than unity. In our experience it is appropriate to set ε_v such that $1/\varepsilon_v = 10Re$, where $Re = \rho UL/\mu$ is the Reynolds number.

In (13), the vector normal to the free surface is required to calculate the velocity gradient in that direction. This does not mean that the exact position of the interface must be known. The fractional volume of liquid can be used to find the normal vector of the interface without knowing its exact position. In each MasCV, the fractional volume of liquid at the corresponding vertex node is defined as the ratio of the liquid volume to its total volume. As with the pressure, the distribution of the fractional volume is interpolated linearly over each primary element. The interfacial pressure is first calculated in each sub-element associated with a filled SMasCV and then an average is taken at the vertex node according to the following procedures. For each filled SMasCV, the gradient of the fractional volume of liquid, ∇f, in the associated primary element is taken and normalized by its own magnitude. The average of these normalized vectors associated with the same vertex node is taken as the inward vector $\mathbf{n}$, which is perpendicular to the free surface. If the air pressure p_0, is taken as zero, then the interfacial pressure in each subelement within a filled SMasCV can be expressed as

$$p = 2\mu_l(\mathbf{n} \cdot \nabla)(\mathbf{v} \cdot \mathbf{n}). \tag{27}$$

After the interfacial pressure in every filled SMasCV is obtained, the average is taken as the interfacial pressure at the vertex node. Since the interfacial pressure is calculated for the liquid, which is incompressible, it is important that the velocity be divergence-free. This is why the average is taken only among those subelements within the filled SMasCVs. On the other hand, it also explains why the interfacial pressure predicted with the discrete migration scheme is expected to be better than that from the continuous interpolation scheme (23), noting that the former satisfies the incompressibility constraint in the filled SMasCVs more exactly than does the latter.

Pressure in the domain

Based on the assumptions made in this study, the pressure of the pseudo-gas is uniform and taken as the reference pressure. The liquid pressure at the vertex node associated with filled MasCVs can be solved explicitly with the continuity equations (20)–(22) or implicitly using the penalty functions (24) and (25). Therefore, the pressure within an empty or filled MasCV can be determined. However, the incompressibility constraint and the liquid pressure on the interface need further consideration. If some of the SMasCV in an MasCV are filled but the others are not, the vertex node within the MasCV is considered on the interface. Since the interfacial pressure of the liquid on the free surface nodes is determined from the stress balance boundary conditon on the interface in (27), it seems that the continuity equation is unnecessary on the interface. However, the volume of liquid flowing between the filled and partially filled SMasCVs cannot be determined correctly unless the mass conservation of the liquid is satisfied within the filled SMasCVs. In particular, the velocity in a partially filled control volume is actually the average velocity of the liquid and the air. This is one of the major reasons why the predicted velocity in a partially filled MasCV needs to be adjusted to satisfy the incompressibility constraint. In the present approach, the adjustment is made by the following method. At each vertex node on the free surface, two pressures are determined. One is the physical pressure obtained from the free surface boundary condition (27), while the other, which is called the pseudo-pressure, is associated with the incompressibility constraint of the liquid velocity within the filled SMasCVs of a partially filled MasCV. Similar to the physical pressure, the pseudo-pressure is interpolated linearly over a primary element. However, there are two differences between them. First, since the pseduo-pressure is not the physical pressure, it should not affect the liquid pressure and the velocity of the interior nodes. Therefore the pseudo-pressure is excluded when integrating the force of the interior nodes in the momentum equation (26). Secondly, the pseudo-pressure in a primary element is multiplied by a weighting factor equal to the volume fraction of liquid in the SMasCV associated with the pseudo-pressure node. This weighting factor enforces the influence of the pseudo-pressure on the liquid velocity perpendicular to the interface. As with the physical pressure at the interior nodes, the pseudo-pressure can be determined explicitly with the continuity equation or implicitly using the penalty function method.

Iteration procedure

The solution procedures can be divided into three parts, namely the initial guess, the following corrections and the criterion of convergence. In addition, there are two convergence criteria, namely one for the status of the SMasCVs and the other for the non-linear advective terms. During each time step, either the initial condition for the first time step or the result from the end of the previous time step is taken as the initial guess. As shown in the block diagram in

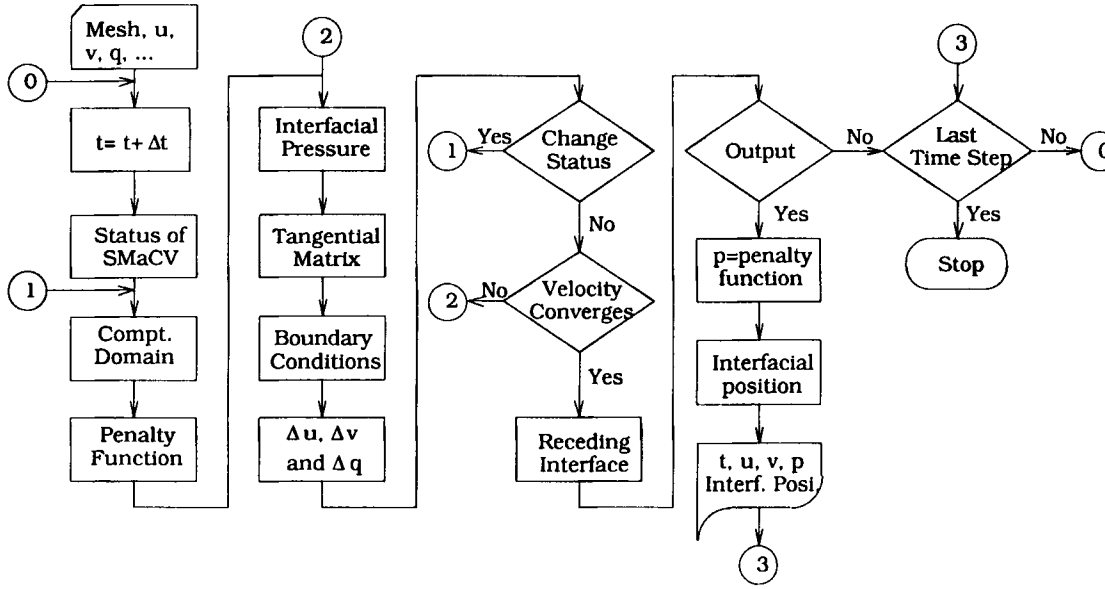

Figure 5. Iteration procedure for net inflow method

Figure 5, when using the penalty function approach, only the incremental velocity is obtained by using the Newton–Raphson method. The pressure is then calculated after the iteration converges. If the pressure and the continuity equation are explicitly included, on the other hand, then both the incremental pressure and velocity are solved simultaneously. After each iteration the status of the unfilled SMasCVs and computational domain is updated based on the new volume of liquid in each SMasCV. Convergence is reached if none of the SMasCVs becomes filled during the last iteration and the root mean square of the incremental velocity is negligibly small.

Receding free surface

In contrast with the case where the free surface advances, if the free surface recedes, then its new position must have been included in the region where the velocity is divergence-free. Since the volume of liquid that recedes from its original position can always be tracked after convergence is reached, the new position of the receding interface is updated after the iteration is over. After convergence is reached, evidence of a receding interface is indicated if the volume of liquid in an SMasCV becomes negative. This means that part of or all the fluid flowing out from the SMasCV during this time step is actually pseudo-gas but was taken as liquid. This negative volume can be corrected for by subtracting the same amount of liquid from the neighbouring SMasCVs into which the fluid had supposedly flowed.

For instance, let us consider a SMasCV with total volume Q and a negative volume of liquid, $-q$. By checking the velocity along its boundaries with non-zero flowing time, those neighbouring SMasCVs into which the fluid flows can be identified. Let m be the number of these SMasCVs and Δq_i $(i = 1, 2, \ldots, m)$ be the volume of fluid that flowed from the SMasCV with negative liquid volume into each of these SMasCVs during the given time step. The volume of liquid in

these SMasCVs should be corrected as

$$q_i^c = q_i - \frac{\Delta q_i}{\sum_{j=1}^{m} \Delta q_j} q, \tag{28}$$

where superscript 'c' denotes the corrected volume of liquid. After the above correction is made, the negative volume of liquid is set to zero.

NUMERICAL EXAMPLES

Several two-dimensional examples have been analysed with the net inflow method. These include the radial planar flow from a point source and the collapse of a water column on either a dry bed or still water. The numerical results are compared with analytical solutions, experimental measurements and/or other numerical solutions whenever available.

Radial planar flow near a point source

As shown in Figure 6, the free surface flow in a rectangular domain near a point source in two-dimensional space is considered. The liquid with constant density $\rho = 1$ and constant velocity viscosity $\mu = 0.1$ flows out from a two-dimensional point source with volumetric flow rate $Q = 2\pi$. The problem is one-dimensional in cylindrical co-ordinates but two-dimensional in rectangular co-ordinates. For convenience, the volumetric flow rate from the point source as well as the size and location of the rectangle are chosen such that both the characteristic velocity and length are one. The analytical solution in cylindrical co-ordinates is given by

$$r_p = \sqrt{(2t)}, \qquad u_r = \frac{1}{r}, \qquad p = \frac{-2\mu}{r_p^2} + \tfrac{1}{2}(r_p^{-2} - r^{-2}), \tag{29}$$

where r_p, u_r and p denote the position of the interface, the radial velocity and the liquid pressure respectively. The time t, is measured from the moment when the liquid begins to flow out from the point source; r is the radial distance from the point source. The analytical solution for the

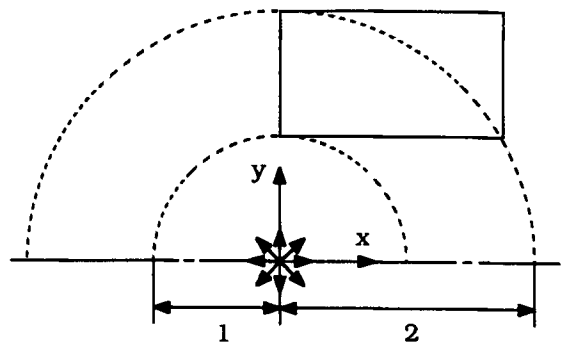

Figure 6. Schematic diagram of radial planar flow near a point source

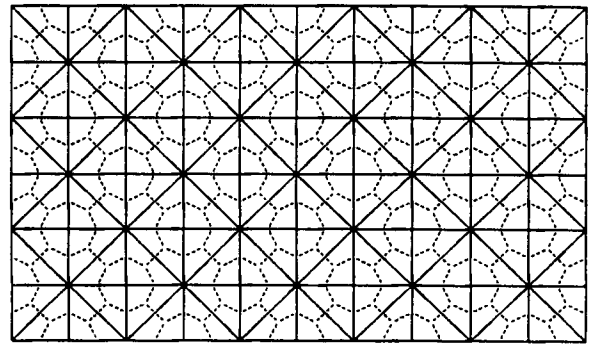

Figure 7. 120-element mesh used to analyse radial flow in rectangular domain indicated in Figure 6

velocity is used as boundary conditions, including the effective flowing time, along the left and bottom of the rectangular domain. The initial condition is $u = v = 0$ within the domain and the penalty parameter is 10^{-6}. In order to understand the dependence of the numerical solution on the mesh size and mesh type, the problem has been solved with three finite element models incorporating 120, 480 and 488 elements respectively. As shown in Figure 7, the domain has been divided into 6×10 uniform rectangles such that the aspect ratio of each rectangle is approximately one. Each rectangle is further divided into two triangular elements and the total number of triangular elements is 120. The dashed lines represent the boundaries of the mass control volumes (MCVs). Similarly, in the 480-element model, the domain is divided into 12×20 uniform rectangles and each rectangle is divided into two triangular elements. As seen in Figure 7, although the domain can be discretized conveniently with a regular mesh, the resulting sizes of the MCVs are non-uniform. In order to test the effect of these non-uniform MCVs, we also solve the problem with a 488-element mesh, as shown in Figure 8, generated using a commercial mesh generator.[25] In particular, the angles of most of the triangular elements in Figure 8 are equal to or close to 60°. As a result, the sizes of most of the MCVs are similar to each other, except for those associated with the domain boundary. The predicted free surface positions, the pressure history at (0, 1) and the pressure distributions are shown in Figures 9–12.

The free surface positions (which have been taken to correspond to where the fractional volume

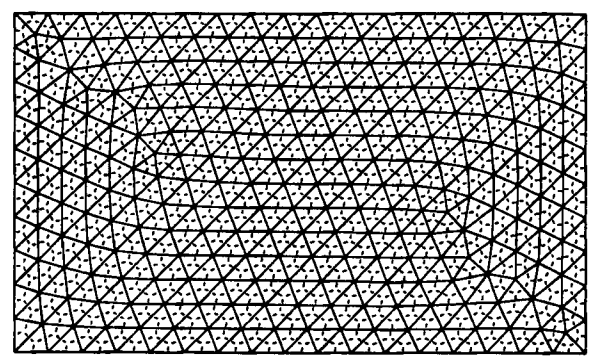

Figure 8. Same as Figure 7 but with 488 elements

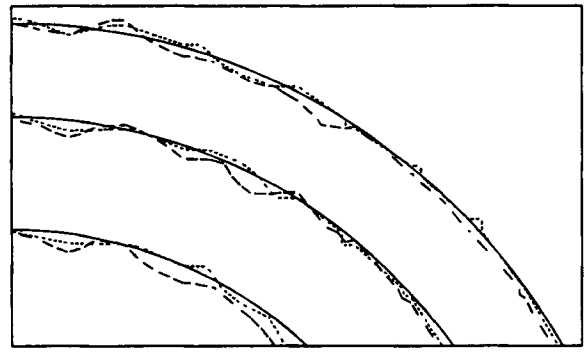

Figure 9. Comparison between free surface positions predicted with 120-element mesh (fine dashed curve: CIS; coarse dashed curve: DMS) and analytical solution (solid curve) for radial planar flow at $t = 0{\cdot}9$, $1{\cdot}4$ and $1{\cdot}9$ s

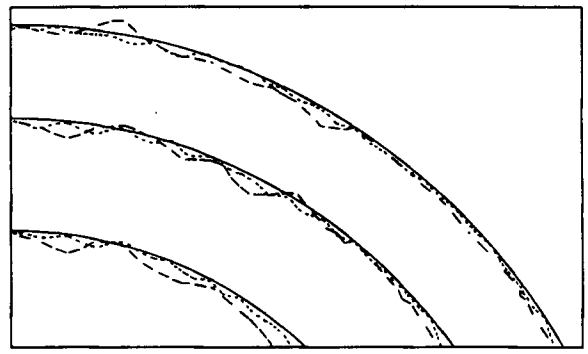

(A)

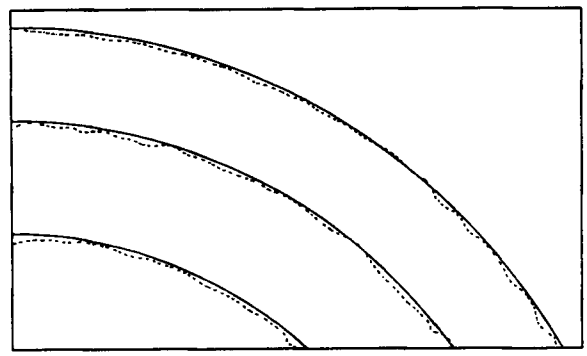

(B)

Figure 10. Comparison between analytical solution (solid curve) and free surface positions for radial planar flow predicted with (A) 120 elements (coarse dashed curve) and 480 elements (fine dashed curve) and (B) 488 elements (dashed curve) at $t = 0{\cdot}9$, $1{\cdot}4$ and $1{\cdot}9$ s, all obtained using DMS

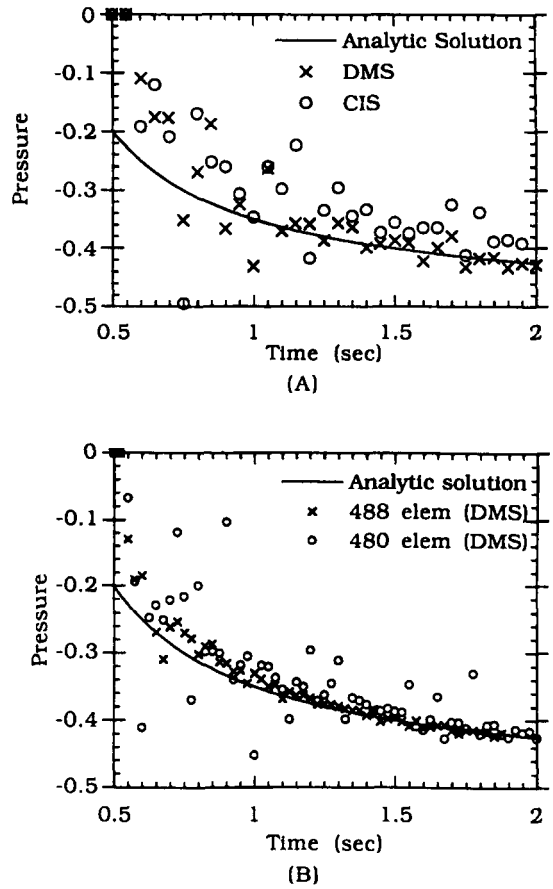

Figure 11. Pressure history at (0, 1) for radial planar flow predicted with (A) 120 elements and (B) 480 and 488 elements

is 0·5) predicted with the 120-element mesh using the discrete migration scheme (DMS) and the continuous interpolation scheme (CIS) have been compared with the analytical solution in Figure 9. The free surface position predicted with the CIS is better than that obtained with the DMS, since the CIS allows a smooth transition in the incompressibility constraint of the liquid velocity near the interface. However, in both cases the deviation between the numerical predictions and the analytical solution seems to be 'wavy'. Furthermore, the deviation is larger when the interface moves in the 90° direction, in which the uniformity of the MCVs is more significant than it is in the 45° direction. By comparing the predicted free surface position with that obtained with the 480-element mesh, as shown in Figure 10(A), it can be seen that both the 'amplitude' and 'period' of the deviation reduce significantly when the mesh size is refined. On the other hand, with approximately the same number of elements, it can be seen in Figure 10(B) that the free surface position predicted with the 488-element mesh is smoother than that obtained with the 480-element mesh.

For the pressure prediction it can be seen from Figures 11(A) and 12(A) that the pressure obtained with the DMS is better, especially near the free surface. This is because the liquid pressure near the interface is closely related to the velocity in (27) and the velocity predicted with the DMS satisfies the incompressibility constraint within the filled SMasCVs more exactly

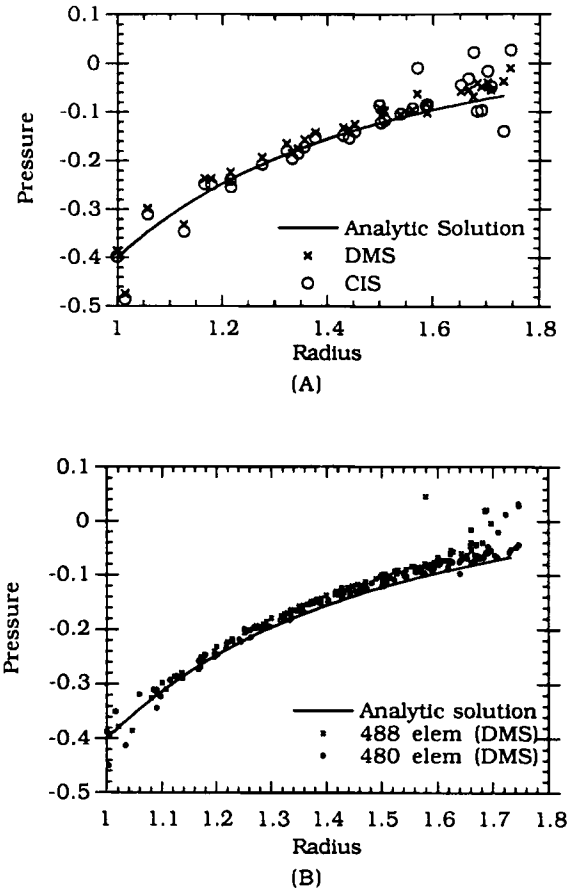

Figure 12. Pressure distribution for radial planar flow at $t = 1{\cdot}5$ s predicted with (A) 120 elements and (B) 480 and 480 elements

than with the CIS. As shown in Figures 11(B) and 12(B), the deviation between the predicted pressure distributions and the analytical solution can be reduced by refining the mesh. Note that in Figure 11(B), the predicted pressure is much smoother with the 488-element mesh where the angle of each element is equal to or close to 60°.

Collapse of a water column on a dry bed

The dam-breaking problem is also known as the collapse of a water column. It includes both advancing and receding motion of the free surface and the experimental data obtained by Martin and Moyce[26] are available for comparison. Similar problems have been studied numerically by Harlow and Welch,[11] Hirt and Nichols[13] and Huerta and Liu.[10] In order to compare our solution with the experimental result, the water column is chosen to be a 5·715 cm × 5·715 cm (2·25 in × 2·25 in) square column.

As shown in Figure 13(A), the dam is suddenly broken at time $t = 0$ and the water column starts to collapse owing to gravity $g = 9{\cdot}8\ \mathrm{m\ s^{-2}}$. The density of water is $1000\ \mathrm{kg\ m^{-3}}$ and its viscosity is taken to be $0{\cdot}001\ \mathrm{kg\ m^{-1}\ s^{-1}}$. For convenience, the dimensionless time and length

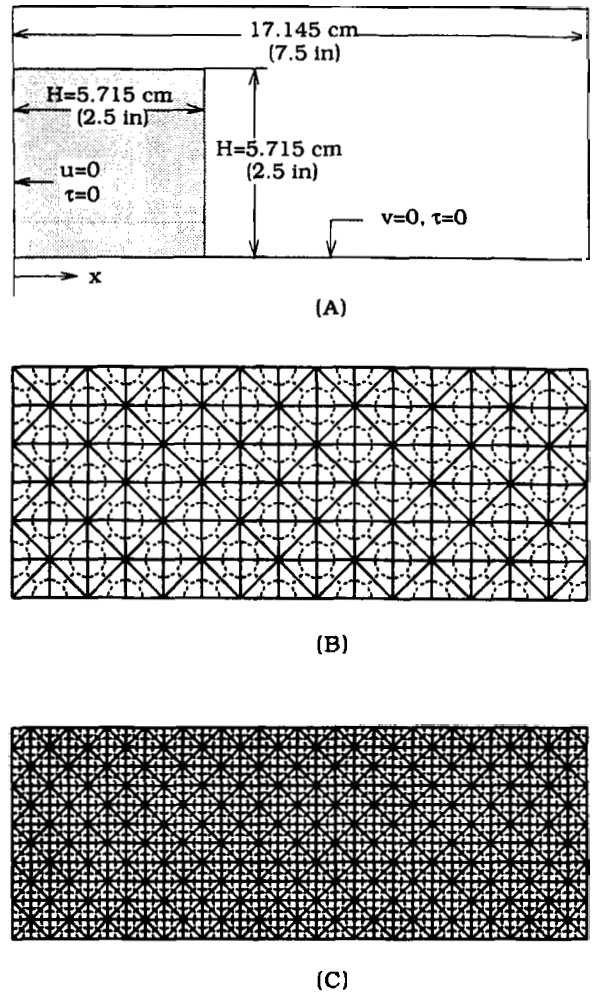

Figure 13. (A) Schematic diagram of collapse of a water column and two finite element configurations corresponding to (B) 180 uniform elements and (C) 660 uniform elements

are defined as $T = t\sqrt{(g/H)}$ and $X = x/H$ respectively. A 6 × 15 mesh and an 11 × 30 mesh, shown in Figures 13(B) and 13(C) respectively, have been used to test the finite element program. A constant time step $\Delta T = 0{\cdot}1$ has been used with the 6 × 15 mesh. For the 11 × 30 mesh ΔT is 0·05 during the first 15 steps. As the water accelerates during the collapse, a smaller $\Delta T = 0{\cdot}025$ has been used during the following 30 time steps. The penalty parameter ε_p has been taken to be $1{\cdot}0 \times 10^{-6}$. The initial condition is $u = v = 0$ everywhere and the elements within the column are occupied by water. The continuity equation is integrated with the discrete migration method and the predicted position of the free surface along the dry bed is compared with Martin and Moyce's experimental results[26] in Figure 14. The solution obtained with the 6 × 15 uniform mesh starts out in good agreement with the measurements until $T \approx 0{\cdot}9$. The subsequent deviation is due to the reduced thickness of the water layer along the bed and the relative coarseness of the mesh. After the mesh is refined, the comparison is significantly improved. The free surface positions and the liquid velocities at each node

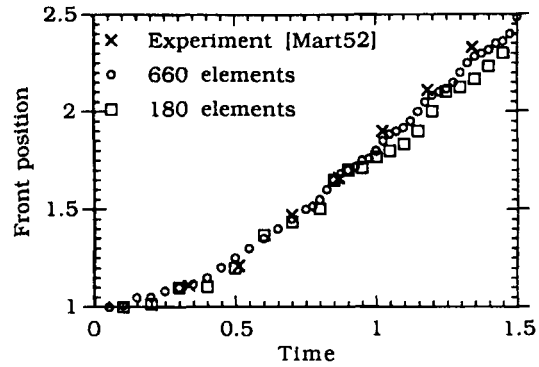

Figure 14. Front position x/H versus time $T = t\sqrt{(g/H)}$ along dry bed during collapse of water column

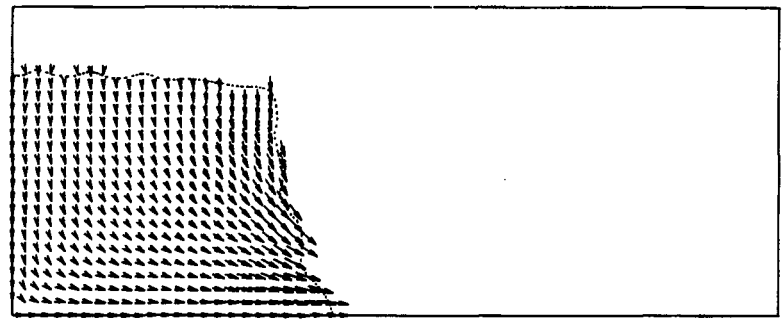

Figure 15. Predicted free surface position (dashed curve) and velocity of water at $T = 0{\cdot}5$ based on mesh with 660 elements

obtained with the 11 × 30 non-uniform mesh at $T = 0{\cdot}5$, $1{\cdot}0$ and $1{\cdot}5$ are shown in Figures 15–17 respectively.

Dam-breaking waves on a still liquid

Unlike the previous example, when a dam collapses on a still liquid, waves are generated owing to the sudden change in depth of the liquid. Since the dam is assumed to break instantaneously, the acceleration of the liquid along the dam surface is infinite at time $t = 0$. This singularity can be removed by assuming the slope of the dam to be finite. Since the liquid velocity and the deformation of the free surface are large near the leading wave but very small both upstream and downstream, the problem can be used to test the numerical stability,[10] especially for a fixed mesh method with non-uniform control volumes. In order to verify our prediction, the problem is defined according to the specifications given by Huerta and Liu,[10] with the exception that the dam is taken to be vertical in the present calculation. As shown in Figure 18, the depth of the still water is 25% of the total depth of the dam, which is 20 m. The density and viscosity of the liquid are $1600\,\mathrm{kg\,m^{-3}}$ and $1000\,\mathrm{Pa\,s^{-1}}$ respectively. In our numerical analysis the domain has been divided into 9 × 40 uniform rectangles, as shown in Figure 19. In this case the continuity equation has been integrated with the continuous interpolation scheme and the time step Δt is $0{\cdot}15\sqrt{(H/g)}$, where $H = 15$ m and $g = 9{\cdot}8\,\mathrm{m\,s^{-2}}$.

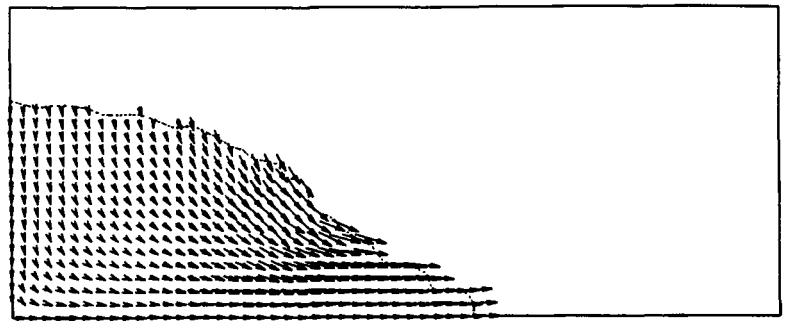

Figure 16. Same as Figure 15 but at $T = 1{\cdot}0$

Figure 17. Same as Figure 15 but at $T = 1{\cdot}5$

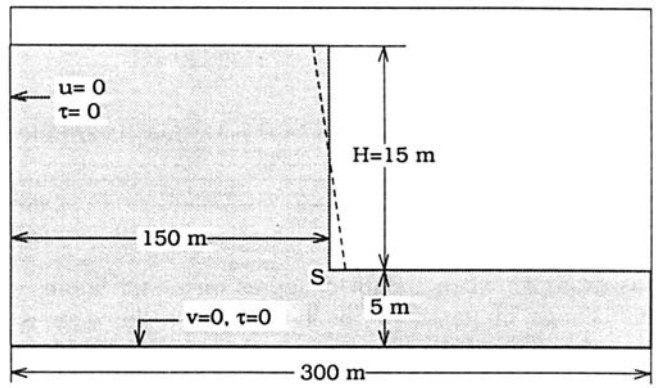

Figure 18. Schematic diagram of dam-breaking problem on still liquid. Dashed line denotes dam assumed by Huerta and Liu[10]

The predicted free surface positions at $T = 1{\cdot}5$, 3, $4{\cdot}5$ and 6, where $T = t\sqrt{(H/g)}$ is the dimensionless time, are shown in Figures 20–23 respectively. Also shown are the free surface positions obtained by Huerta and Liu[10] with their arbitrary Lagrangian–Eulerian method at $T = 3$ and 6 in Figures 21 and 23 respectively. In Figure 20 the liquid immediately in front of the broken dam is pushed upwards and forwards by a large pressure gradient while the water column collapses. It should be noted that the scales are different in the horizontal and vertical

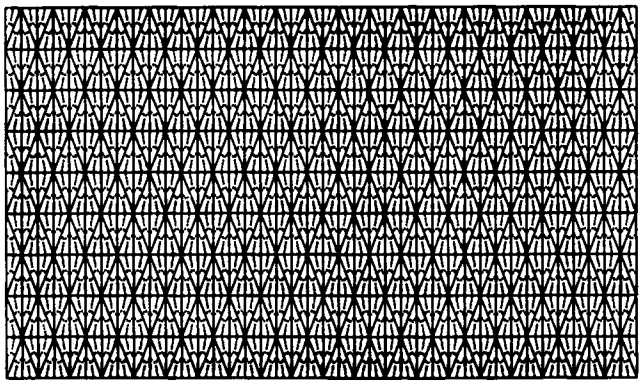

Figure 19. Finite elements for dam-breaking problem on still liquid. Dashed lines are boundaries of mass control volumes

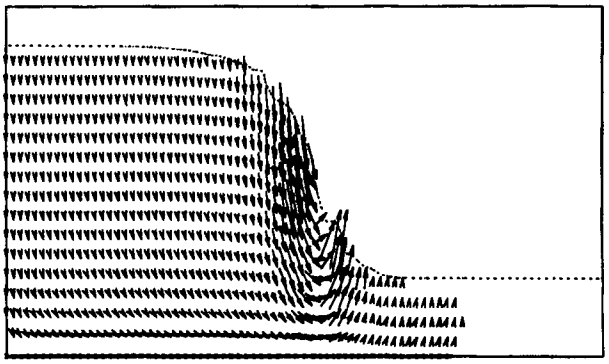

Figure 20. Predicted free surface position and velocity of dam-breaking problem on still water at $T = 1{\cdot}5$

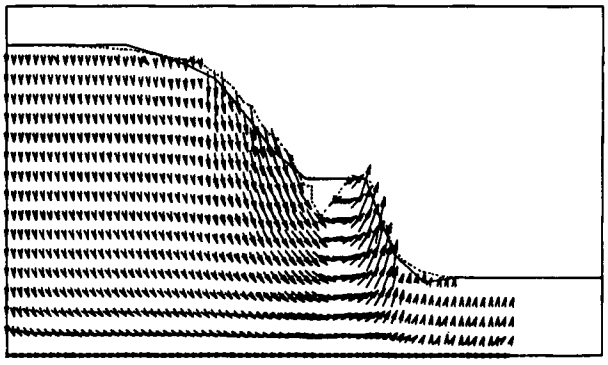

Figure 21. Predicted free surface position (dashed curve) and velocity of dam-breaking problem on still water at $T = 3$. Solid curve denotes free surface position predicted by Huerta and Liu[10]

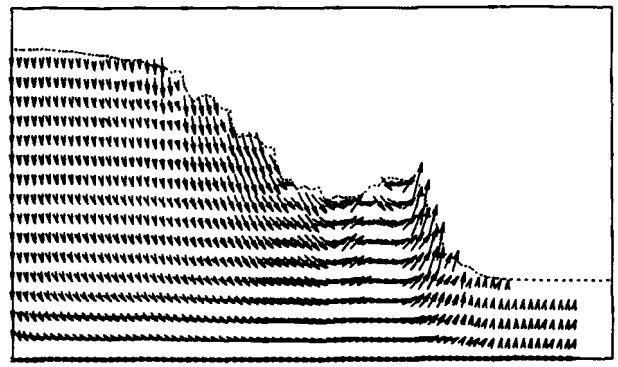

Figure 22. Same as Figure 20 but at $T = 4{\cdot}5$

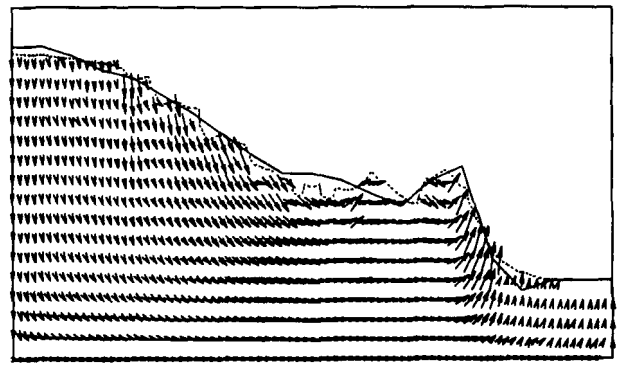

Figure 23. Same as Figure 21 but at $T = 6$

directions. In Figure 21, a leading wave has formed and moved forwards. The plateau-like wave shape in Huerta and Liu's solution[10] is believed to be related to the coarse mesh and initial 1:1 slope assumed in their calculation. As shown in Figures 22 and 23, when the leading wave moves forwards, a series of secondary waves with smaller wavelength and amplitude form and follow behind the leading wave. Apparently, the shape and motion of these secondary waves can only be predicted accurately with a finer mesh with uniform MCVs. However, the amplitude, shape and position of the travelling wave predicted with the regular mesh are seen to agree closely with those of Huerta and Liu's result.[10]

CONCLUSIONS

A new control volume finite element procedure called the net inflow method as been developed to simulate time-dependent incompressible viscous flow with moving free surfaces in two-dimensional space. The 2D Navier–Stokes equations in primary variables (velocity and pressure) are solved with a fixed mesh approach, so that problems with irregular geometry can be considered. The method is efficient, since only the region occupied by the liquid and a layer of air near the interface are included in the computational domain. The CPU time can be further reduced by incorporating the penalty function method. Since the resolution of the predicted

interfacial position is closely related to the conservation of mass near the free surface, each mass control volume is divided into several sub-mass control volumes. For a given mesh the flexible combination of these sub-mass control volumes gives much better resolution than the whole mass control volumes in fitting the irregular shape of the free surface. Near the free surface, the continuity equation of the liquid can be integrated discretely in the filled sub-mass control volumes or continuously with a special interpolation method. No material marker or additional kinetic equation is required to track the interfacial position. During the iteration the exact position of the interface does not have to be determined and the free surface boundary conditions are satisfied on the interfacial nodes determined based on the status (filled or non-filled) of the submass control volumes. The method has been used to analyze several free surface flow problems.[17] The examples presented in this paper show that the net inflow method is stable, efficient and can be applied in the analysis of general 2D incompressible free surface flow problems including inertial effects.

ACKNOWLEDGEMENT

The authors thank Dr. C. A. Hieber and Professor S. F. Shen for their valuable comments and discussions. This project is supported by the National Science Foundation under Grant 8815855. The computations were carried out using the Cornell National Supercomputer Facility.

REFERENCES

1. J. E. Welch, F. H. Harlow, J. P. Shannon and B. J. Daly, 'The MAC method,' *Los Alamos Scientific Laboratory Rep. LA-3425*, (1965).
2. R. E. Nickell, R. I. Tanner and B. Caswell. 'The solution of viscous incompressible jet and free surface flows using finite element methods,' *J Fluid Mech.*, **65**, 189–206 (1974).
3. B. J. Omodei, 'Computer solutions of plane Newtonian jet with surface tension,' *Comput. Fluids*, **7**, 79–96 (1979).
4. W. J. Silliman and L. E. Scriven, 'Separating flow near a static contact-line: slip at a wall and shape of a free surface,' *J Comput. Phys.*, **34**, 287–313 (1980).
5. K. J. Ruschak, 'A method of incorporating free boundaries with surface tension in finite element fluid-flow simulators,' *Int. j. numer. methods eng.*, **15**, 639–648 (1980).
6. H. Saito and L. E. Scriven, 'Study of coating flow by the finite element method,' *J. Comput. Phys.*, **42**, 53–76 (1981).
7. G. Ryskin and L. G. Leal, 'Numerical solution of free-boundary problems in fluid mechanics. Part 1, The finite-difference technique,' *J Fluid Mech.*, **148**, 1–17 (1984).
8. H. S. Kheshgi and L. E. Scriven, 'Penalty-finite element analysis of time-dependent two-dimensional free surface film flow,' T. Kawai (ed.), *Finite Element Flow Analysis, Proc. Fourth Int. Symp. on Finite Element Methods in Flow Problems*, University of Tokyo Press, Tokyo, 1982, pp. 113–120.
9. W. F. Noh, 'CEL: a time-dependent two-space-dimensional coupled Eulerian–Langrangian code,' in B. A. S. Fernbach and M. Rotenberg (eds), *Methods in Computational Physics*, Vol. 3, 1964, pp. 117–179.
10. A. Huerta and W. K. Liu, 'Viscous flow with large free surface motion,' *Comput. Methods Appl. Mech. Eng.*, **69**, 277–324 (1988).
11. F. H. Harlow and J. E. Welch, 'Numerical calculation of time-dependent viscous incompressible flow of fluid with free surface,' *Phys. Fluids*, **8**, 2182–2189 (1965).
12. E. Broyer, C. Gutfinger and Z. Tadmore, 'A theoretical model for the cavity filling process in injection molding,' *Trans. Soc. Rehol.*, **19**, 423–444 (1975).
13. C. W. Hirt and B. D. Nichols, 'Volume of fluid (VOF) method for the dynamics of free boundaries,' *J Comput. Phys.*, **39**, 201–225 (1981).
14. B. R. Baliga and S. V. Patankar, 'A control volume finite-element method for two-dimensional fluid flow and heat transfer,' *Numer. Heat Transfer*, **6**, 245–261 (1980).
15. C. Prakash, 'Examination of the upwind (donor-cell) formulation in control volume finite-element methods for fluid flow and heat transfer,' *Numer Heat Transfer*, **11**, 401–416 (1987).
16. G. E. Schneider and M. J. Raw, 'A skewed, positive influence coefficient upwinding procedure for control-volume-based finite element convection–diffusion computaton,' *Numer Heat Transfer*, **9**, 1–26 (1986).
17. S. P. Wang, 'Numerical simulation and experiment of incompressible viscous flow with moving free surfaces,' *Ph.D. Thesis*, Cornell University, Ithaca, NY, 1992.
18. S. V. Patankar, *Numerical Heat Transfer and Fluid Flow*, MacGraw-Hill, New York, 1980.

19. O. C. Zienkewicz, R. L. Taylor and J. M. Too. 'Reduced integration technique in general analysis of plates and shells,' *Int. J. numer. methods eng.*, **3**, 575–586 (1971).
20. T. J. R. Hughes, W. K. Liu and A. Brooks, 'Finite element analysis of incompressible viscous flows by the penalty function formulation,' *J Comput. Phys.*, **30**, 1–60 (1979).
21. M. S. Engelman, R. I. Sani, P. M. Gresho and M. Bercovier, 'Consistent vs. reduced integration penalty methods for incompressible media using several old and new elements,' *Int. j. numer. methods fluids*, **2**, 25–42 (1982).
22. G. F. Carey and R. Krishnan, 'Penalty finite element method for the Navier–Stokes equation,' *Comput. Methods Appl. Mech. Eng.*, **42**, 183–224 (1984).
23. H. S. Kheshgi and L. E. Scriven, 'Variable penalty method for finite element analysis of incompressible flow,' *Int. j. numer. methods fluids*, **5**, 785–803 (1985).
24. M. Iga and J. N. Reddy, 'Penalty finite element analysis of free surface flows of power-law fluids,' *Int. J. Non-linear Mech.*, **24**, 383–399 (1989).
25. C-MOLD User's Manual, Advanced CAE Technology, Ithaca, NY, 1993.
26. J. C. Martin and W. J. Moyce, 'An experimental study of the collapse of liquid columns on a rigid horizontal plane,' *Philos. Trans. Ser. A, Math. Phys. Sci.*, **244**, 312–324 (1952).